Comput Mech (2009) 44:621–630
DOI 10.1007/s00466-009-0397-0

ORIGINAL PAPER

A finite strain framework for the simulation of polymer curing. Part I: elasticity

M. Hossain · G. Possart · P. Steinmann

Received: 23 February 2009 / Accepted: 7 May 2009 / Published online: 24 May 2009

Abstract A phenomenologically motivated small strain model to simulate the curing of thermosets has been developed and discussed in a recently published paper (Hossain et al. in Comput Mech 43(6):769–779, 2009). Inspired by the concepts used there, this follow-up contribution presents an extension towards the finite strain regime. The thermodynamically consistent framework proposed here for the simulation of curing polymers particularly is independent of the choice of the free energy density, i.e. any phenomenological or micromechanical approach can be utilised. Both the governing equations for the curing simulation framework and the necessary details for the numerical implementation within the finite element method are derived. The curing of polymers is a very complex process involving a series of chemical reactions typically resulting in a conversion of low molecular weight monomer solutions into more or less cross-linked solid macromolecular structures. A material undergoing such a transition can be modelled by using an appropriate constitutive relation that is distinguished by prescribed temporal evolutions of its governing material parameters, which have to be determined experimentally. Part I of this work will deal with the elastic framework whereas the following Part II will focus on viscoelastic behaviour and shrinkage effects. Some numerical examples demonstrate the capability of our approach to correctly reproduce the behaviour of curing materials.

M. Hossain · G. Possart · P. Steinmann (✉)
University of Erlangen-Nuremberg,
Egerlandstraße 5, 91058 Erlangen, Germany
e-mail: paul.steinmann@ltm.uni-erlangen.de

M. Hossain
e-mail: mokarram.hossain@ltm.uni-erlangen.de

G. Possart
e-mail: gunnar.possart@ltm.uni-erlangen.de

Keywords Curing · Polymer · Finite strains · Elasticity

1 Introduction and previous work

There is a vast number of applications in almost every branch of daily life where polymeric materials play an important role. In cases where the very formation of such materials plays a decisive role to meet particular design goals of a structure, e.g. for adhesives in automotive, electronics or aerospace industry, one can observe an increasing demand for constitutive models and simulation methods that consider a time- or degree of cure dependence of the mechanical properties. Apart from adhesives, further applications relevant for such models would be carbon- or glass fibre-reinforced epoxy laminates and (nano-)particle-reinforced polymer structures in general.

An uncured polymer usually behaves as a deformable viscous liquid practically incapable of sustaining any load other than hydrostatic. With time evolving, the curing reactions proceed, polymer chains form (and possibly cross-link to each other) and the viscosity of the liquid resin, its molecular weight and the stiffness increase. A number of rheological analogies to such processes have been applied and discussed by several authors [1–4] and also our previous small strain curing model made extensive use of such assumptions. Since some review on available literature and modelling approaches concerning the curing of polymers has been given already in [5], we omit further details on this here and refer only to the general purpose finite strain curing models known to us so far.

A physically and chemically sound approach to model polymer curing has been developed in a series of papers by Adolf and co-workers [2,6–9], who proposed not only linear constitutive models but also an extension to the large

strain regime. Their continuum model, originally devised to describe viscoelastic glassy polymers, is extended towards the curing of polymers by the introduction of an additional dependent variable into the Helmholtz free energy, namely the completion of reaction. The only limitation of this model is that it is not formulated in a way suitable to implementation within the finite element framework, i.e. a full derivation of stress tensors and consistent tangent operators, which are essential for the iterative solution of boundary value problems within finite element schemes, is lacking.

Another approach has recently been published by Lion and Höfer [1] who proposed a phenomenological thermo-viscoelastic curing model for finite strain deformations. It accounts for thermally and chemically induced volume changes via a ternary multiplicative split of the deformation gradient into mechanical, thermal and chemical parts. Similar to Adolf's ansatz, a coordinate of reaction is introduced that corresponds to the degree of cure. The model is mainly based on the assumption of process dependent viscosities as in the previous works of Haupt and Lion [10–12]. The resulting constitutive relation is derived in a thermodynamically consistent manner, i.e. it fulfills the second law of thermodynamics, which is an important issue that many of the earlier curing models did not touch. Detailed algorithmic formulations for the finite element implementation of this model are elaborated in Retka and Höfer [13]. The energy density used for the mechanical part of this model is of a phenomenological type. Although the authors claim this model to be independent concerning the choice of energy density it seems somehow complicated to derive stresses and tangent operators in case that different constitutive models are applied.

2 Main concepts and outline

The main assumption, considered earlier [5] in the development of linear constitutive curing models, is, from the rheological point of view, that a cross-linking or curing process can, for the elastic case, be understood as a continuous increase in stiffness. From a molecular point of view we assumed further that when a step in strain is applied, the chains between existing cross-links are deformed which is accompanied by some stress distribution in the material. Due to the progress in curing, new cross-links occur which has been conceptualised by the addition of new chains to the network. These fit into the already deformed structure and are not affected by the previous deformation, i.e. new chains do not contribute to the stress until the deformation is changed again. Expressed in rates this behaviour would be described by $\dot{\boldsymbol{\sigma}} = \mathbf{0}$ as long as $\dot{\boldsymbol{\varepsilon}} = \mathbf{0}$. It is noteworthy that this particular behaviour prohibits the simulation of curing materials by just considering an additional time dependence of the material parameters. If, on the other hand, (thermo-)viscoelastic formulations governed only by process dependent viscosities are used as in Lion's approach [1], this property is intrinsically captured. Since we would like to avoid any initial restriction concerning the choice of constitutive model, we depart from our general equation for the stress update developed in [5] and provide the necessary extensions to capture finite strain deformations. The resulting simulation framework for elastically curing materials entirely captures the above mentioned requirements, except for thermally induced effects which will be treated later. Furthermore, this approach is valid only for materials that have passed the gel point, which is only a weak restriction since the stiffness increase relevant for practical applications takes place mainly after gelation. In particular, we will omit the consideration of the initial polymer solution as a multi-component diffusion mixture.

This paper is organised as follows: Sect. 3 develops the necessary equations for the three-dimensional finite strain curing simulation framework by extending the one-dimensional main equation that originated from simple rheological considerations. In Sect. 4, the simulation framework is particularised for two different energy density functions, which are the phenomenological compressible Neo-Hookean material and the micro-mechanical 21-chain unit-sphere model. After the details of the numerical implementations within the finite element method have been derived, Sect. 5 discusses the required cure-dependent material parameter evolutions which is followed by a final Sect. 6 presenting some numerical examples.

3 General simulation framework

The method introduced here aims at the simulation of materials undergoing finite strain deformations while their elastic properties are simultaneously experiencing a temporal evolution. As discussed above such a simulation framework is of particular interest if e.g. curing phenomena typically appearing in polymer materials have to be considered. As a starting point we go back to the general equation for the one-dimensional stress update of our recently published [5] small strain modelling approach for the curing of thermosets:

$$\dot{\sigma}(t) = c(t)\dot{\varepsilon}(t). \tag{1}$$

Thereby, $c(t)$ denotes the time-dependent material stiffness linearly relating stress- and strain-rate. For the case of large strain deformations we transfer this format to

$$\dot{\boldsymbol{S}}(t) = \mathbb{C}(t) : \dot{\boldsymbol{E}}(t) = \frac{1}{2}\mathbb{C}(t) : \dot{\boldsymbol{C}}(t), \tag{2}$$

where $\boldsymbol{S}$, $\boldsymbol{E} = \frac{1}{2}[\boldsymbol{C} - \boldsymbol{I}]$ and $\boldsymbol{C}$ denote the 2nd Piola-Kirchhoff stress tensor, the Green-Lagrange strain tensor and the right

Cauchy-Green tensor, respectively. By $(\dot{\bullet})$ the material time derivative is expressed and $\mathbb{C}(t)$ describes the time dependent *stiffness operator* as derived from the strain energy density Ψ of an arbitrary, time-dependent material model via

$$\mathbb{C}(t) = 4\frac{\partial^2 \Psi(t)}{\partial \boldsymbol{C}^2(t)}. \tag{3}$$

Stress formulation (2) is of a hypoelastic type, although it differs from the original version proposed by Truesdell and Noll [14]. As for any other constitutive assumption, the property of thermodynamical consistency requires special attention. This property is given if a free energy density Φ can be formulated that satisfies the isothermal dissipation inequality

$$\boldsymbol{S} : \dot{\boldsymbol{E}} - \dot{\Phi} \overset{!}{\geq} 0 \tag{4}$$

for all possible processes. The standard Coleman-Noll argumentation then provides the stress formulation (2) if the following ansatz for Φ is chosen:

$$\Phi(t) = \frac{1}{2}\int_0^t \left[\mathbb{C}'(s) : [\boldsymbol{E}(t) - \boldsymbol{E}(s)]\right] : [\boldsymbol{E}(t) - \boldsymbol{E}(s)] ds, \tag{5}$$

where $\mathbb{C}'(s) = d\mathbb{C}(s)/ds$ denotes the total differential of the material specific, time dependent stiffness tensor according to Eq. (3) and with respect to the integration variable s. In analogy to a linear spring, this convolution integral can be interpreted as the accumulation of elastically stored energy while both the stiffness and the deformation are continuously evolving. Note that definition (5) is physically reasonable if and only if the derivative of the stiffness tensor is positive semi-definite, i.e.

$$[\mathbb{C}' : \boldsymbol{E}] : \boldsymbol{E} \geq 0 \quad \forall \boldsymbol{E}, \tag{6}$$

which is a requirement intrinsically met if $\mathbb{C}$ is derived from an appropriately chosen strain energy density Ψ.

To evaluate the dissipation inequality (4) the material time derivative $\dot{\Phi}$ needs to be computed:

$$\begin{aligned}
\dot{\Phi} &= \frac{1}{2}\left[[\mathbb{C}'(s) : [\boldsymbol{E}(t) - \boldsymbol{E}(s)]] : [\boldsymbol{E}(t) - \boldsymbol{E}(s)]\right]_{s=t} \\
&\quad + \frac{1}{2}\int_0^t \frac{\partial}{\partial t}\left([\mathbb{C}'(s) : [\boldsymbol{E}(t) - \boldsymbol{E}(s)]] : [\boldsymbol{E}(t) - \boldsymbol{E}(s)]\right) ds \\
&= 0 + \frac{1}{2}\int_0^t [\mathbb{C}'(s) : \dot{\boldsymbol{E}}(t)] : [\boldsymbol{E}(t) - \boldsymbol{E}(s)] ds \\
&\quad + \frac{1}{2}\int_0^t [\mathbb{C}'(s) : [\boldsymbol{E}(t) - \boldsymbol{E}(s)]] : \dot{\boldsymbol{E}}(t) ds \\
&= \left[\int_0^t \mathbb{C}'(s) : [\boldsymbol{E}(t) - \boldsymbol{E}(s)]\right] : \dot{\boldsymbol{E}}(t) ds.
\end{aligned} \tag{7}$$

The last equality sign requires permutability of the double contractions, i.e.

$$\begin{aligned}
&[\mathbb{C}' : \boldsymbol{A}] : \boldsymbol{B} = [\mathbb{C}' : \boldsymbol{B}] : \boldsymbol{A} \quad \forall \boldsymbol{A}, \boldsymbol{B} \\
&\Leftrightarrow \quad (\mathbb{C}')_{ijkl} A_{kl} B_{ij} = (\mathbb{C}')_{klij} B_{ij} A_{kl},
\end{aligned} \tag{8}$$

which is given since $\mathbb{C}$ stems from a potential and thus possesses major symmetry. Insertion of result (7) into the elastic version of (4) yields

$$\left[\boldsymbol{S}(t) - \int_0^t \mathbb{C}'(s) : [\boldsymbol{E}(t) - \boldsymbol{E}(s)] ds\right] : \dot{\boldsymbol{E}}(t) \overset{!}{=} 0 \tag{9}$$

and the standard Coleman-Noll procedure provides the following functional for the 2nd Piola-Kirchhoff stress:

$$\boldsymbol{S}(t) = \int_0^t \mathbb{C}'(s) : [\boldsymbol{E}(t) - \boldsymbol{E}(s)] ds. \tag{10}$$

Computing the material time derivative finally yields the desired result, i.e. constitutive equation (2):

$$\begin{aligned}
\dot{\boldsymbol{S}}(t) &= \left[\mathbb{C}'(s) : [\boldsymbol{E}(t) - \boldsymbol{E}(s)]\right]_{s=t} + \int_0^t \mathbb{C}'(s) : \dot{\boldsymbol{E}}(t) ds \\
&= \mathbb{C}(t) : \dot{\boldsymbol{E}}(t) = \frac{1}{2}\mathbb{C}(t) : \dot{\boldsymbol{C}}(t).
\end{aligned} \tag{11}$$

This tensor-valued ordinary differential equation for the stress can be solved iteratively by applying numerical integration schemes like the implicit Euler backward:

$$\boldsymbol{S}^{n+1} = \boldsymbol{S}^n + \frac{1}{2}\mathbb{C}^{n+1} : \left[\boldsymbol{C}^{n+1} - \boldsymbol{C}^n\right], \tag{12}$$

whereas $[\bullet]^n = [\bullet](t_n)$ and $t_{n+1} = t_n + \Delta t$. The main advantage of this stress formulation is that any kind of constitutive (polymer) model—either phenomenologically or micromechanically based—can be inserted. The only ingredients required are the temporal evolutions of the governing material parameters to determine $\mathbb{C}^{n+1}$, which can be parametrised e.g. directly in time or in terms of the degree of cure. In particular, this ansatz is not restricted to hyperelasticity but can also be used for viscoelastic material models, as will be discussed in a forthcoming paper. A second important property of relation (12) is its capability to reproduce the physical observation that the stress state of a curing material is changed if and only if its strain state is modified, i.e. $\dot{\boldsymbol{S}} = \boldsymbol{0}$ as long as $\dot{\boldsymbol{C}} = \boldsymbol{0}$. This requirement constitutes a significant design constraint for any model considering curing processes. It assures that the evolution of material properties becomes visible just by the time the deformation state is changed—even though its free energy density evolves permanently.

In order to apply the finite element method for the solution of boundary value problems under certain constitutive

assumptions, it is common practice to resort to implicit iterative schemes like the Newton-Raphson method. In particular, a consistent linearisation of stress formulation (12) with respect to changes in strain is required. The computation of this current *tangent operator* introduces a sixth-order tensor $\mathfrak{A}$, namely the derivative of the current material specific stiffness operator with respect to the strain:

$$\begin{aligned}\mathbb{E}^{n+1} &= 2\frac{\partial \boldsymbol{S}^{n+1}}{\partial \boldsymbol{C}^{n+1}} = \frac{\partial\left(2\boldsymbol{S}^{n}+\mathbb{C}^{n+1}:\left[\boldsymbol{C}^{n+1}-\boldsymbol{C}^{n}\right]\right)}{\partial \boldsymbol{C}^{n+1}}\\ &= \mathbb{C}^{n+1}:\mathbb{I}^{sym}+\left[\boldsymbol{C}^{n+1}-\boldsymbol{C}^{n}\right]:\frac{\partial \mathbb{C}^{n+1}}{\partial \boldsymbol{C}^{n+1}}\\ &= \mathbb{C}^{n+1}+\left[\boldsymbol{C}^{n+1}-\boldsymbol{C}^{n}\right]:\mathfrak{A}^{n+1}, \end{aligned} \tag{13}$$

where $\mathbb{I}^{sym}=\frac{1}{2}[\delta_{ik}\delta_{jl}+\delta_{il}\delta_{jk}]$ denotes the symmetric fourth order identity tensor, δ_{ij} is the Kronecker delta and $\mathfrak{A}^{n+1}=\partial\mathbb{C}^{n+1}/\partial\boldsymbol{C}^{n+1}$. To avoid confusion of time scales, it is worth pointing out that this derivative provides the change of the stiffness operator $\mathbb{C}$, being defined by the governing parameters at a fixed time of curing t_{n+1}, with respect to the current change in strain $\boldsymbol{C}$.

In the following sections, the framework for the simulation of curing materials described above will be particularised for the two cases of a phenomenologically (Neo-Hooke) and a micromechanically (micro-macro-unit-sphere 21-chain model) motivated polymer model. To this end the underlying expressions for free energy density Ψ and stiffness operator $\mathbb{C}$ are recapitulated and the corresponding tangent operators $\mathbb{E}$ are derived.

4 Application to curing of polymers

4.1 Phenomenological example: Neo-Hooke model

We first consider a rather simple but frequently used phenomenological constitutive ansatz for polymers, the so-called compressible Neo-Hooke model for which the corresponding free energy density is given by

$$\Psi(\boldsymbol{C},J)=\frac{1}{2}\kappa(\ln J)^2-\mu\ln J+\frac{1}{2}\mu\left[I_1-3\right]. \tag{14}$$

Here, $I_1=\boldsymbol{C}:\boldsymbol{I}$ denotes the first invariant of the right Cauchy-Green tensor while $J=\det\boldsymbol{F}$ is the determinant of the deformation gradient and κ and μ are the Lamé parameters. Using Eq. (3) some manipulations provide the corresponding stiffness operator $\mathbb{C}$ which is required in Eqs. (12), and (13):

$$\begin{aligned}\mathbb{C} &= 4\frac{\partial^2\Psi}{\partial\boldsymbol{C}^2}\\ &= \kappa\boldsymbol{C}^{-1}\otimes\boldsymbol{C}^{-1}+2\left[\mu-\kappa\ln J\right]\boldsymbol{C}^{-1}\odot\boldsymbol{C}^{-1}\\ &= \kappa\mathbb{A}-2\left[\mu-\kappa\ln J\right]\mathbb{B}. \end{aligned} \tag{15}$$

For a detailed derivation the reader is referred to e.g. [15,16]. The fourth-order tensors $\mathbb{A}$ and $\mathbb{B}$ are introduced for the sake of simplicity and can be written component-wise as

$$(\mathbb{A})_{ijkl}=\left(\boldsymbol{C}^{-1}\otimes\boldsymbol{C}^{-1}\right)_{ijkl}=C^{-1}_{ij}C^{-1}_{kl} \tag{16}$$

$$(\mathbb{B})_{ijkl}=\left(\frac{\partial\boldsymbol{C}^{-1}}{\partial\boldsymbol{C}}\right)_{ijkl}=-\frac{1}{2}\left[C^{-1}_{ik}C^{-1}_{jl}+C^{-1}_{il}C^{-1}_{jk}\right]. \tag{17}$$

Thus, the current stiffness operator necessary to update the stress according to Eq. (12) is determined by the cure-dependent parameters κ, μ and the strain state included in J, $\mathbb{A}$, $\mathbb{B}$:

$$\mathbb{C}^{n+1}=\kappa^{n+1}\mathbb{A}-2\left[\mu^{n+1}-\kappa^{n+1}\ln J\right]\mathbb{B}. \tag{18}$$

The current tangent operator (13) additionally requires the computation of $\mathfrak{A}^{n+1}$:

$$\begin{aligned}\mathfrak{A}^{n+1} &= \frac{\partial\mathbb{C}^{n+1}}{\partial\boldsymbol{C}}\\ &= \kappa^{n+1}\left[\frac{\partial\mathbb{A}}{\partial\boldsymbol{C}}+2\ln J\frac{\partial\mathbb{B}}{\partial\boldsymbol{C}}+\mathbb{B}\otimes\boldsymbol{C}^{-1}\right]-2\mu^{n+1}\frac{\partial\mathbb{B}}{\partial\boldsymbol{C}}\\ &= \kappa^{n+1}\left[\mathfrak{B}+2\ln J\,\mathfrak{C}+\mathbb{B}\otimes\boldsymbol{C}^{-1}\right]-2\mu^{n+1}\mathfrak{C}, \end{aligned} \tag{19}$$

which closes the constitutive equations for a Neo-Hookean material undergoing a curing process. For the sake of completeness the sixth-order tensors $\mathfrak{B}=\mathbb{A}_{,\boldsymbol{C}}$ and $\mathfrak{C}=\mathbb{B}_{,\boldsymbol{C}}$ are given component-wise:

$$\begin{aligned}(\mathfrak{B})_{ijklpq} &= \frac{\partial\left(C^{-1}_{ij}C^{-1}_{kl}\right)}{\partial C_{pq}}=\frac{\partial C^{-1}_{ij}}{\partial C_{pq}}C^{-1}_{kl}+C^{-1}_{ij}\frac{\partial C^{-1}_{kl}}{\partial C_{pq}}\\ &= -\frac{1}{2}\left[C^{-1}_{ip}C^{-1}_{jq}C^{-1}_{kl}+C^{-1}_{iq}C^{-1}_{jp}C^{-1}_{kl}\right.\\ &\quad\left.+\;C^{-1}_{ij}C^{-1}_{kp}C^{-1}_{lq}+C^{-1}_{ij}C^{-1}_{kq}C^{-1}_{lp}\right], \end{aligned} \tag{20}$$

$$\begin{aligned}(\mathfrak{C})_{ijklpq} &= -\frac{1}{2}\frac{\partial\left(C^{-1}_{ik}C^{-1}_{jl}+C^{-1}_{il}C^{-1}_{jk}\right)}{\partial C_{pq}}\\ &= \frac{1}{4}\left[C^{-1}_{ip}C^{-1}_{kq}C^{-1}_{jl}+C^{-1}_{iq}C^{-1}_{kp}C^{-1}_{jl}+C^{-1}_{ik}C^{-1}_{jp}C^{-1}_{lq}\right.\\ &\quad+C^{-1}_{ik}C^{-1}_{jq}C^{-1}_{lp}+C^{-1}_{ip}C^{-1}_{lq}C^{-1}_{jk}+C^{-1}_{iq}C^{-1}_{lp}C^{-1}_{jk}\\ &\quad\left.+C^{-1}_{il}C^{-1}_{jp}C^{-1}_{kq}+C^{-1}_{il}C^{-1}_{jq}C^{-1}_{kp}\right]. \end{aligned} \tag{21}$$

4.2 Micromechanical example: 21-chain model

The utilisation of micromechanically motivated polymer models in curing simulations has the advantage that the temporal evolutions of the governing parameters reflect the microstructural changes taking place in the material during its formation. In particular one frequently encounters parameters like *number of segments per chain* and *number of chains*

per unit volume which have to evolve in opposite directions during curing. For example, a small number of long (and rather soft) chains is successively cross-linked to a network containing a high number of short (and much stiffer) chains, as is discussed in more detail in Sect. 5.

From the number of micromechanical models available in the literature, cf. e.g. [17,18] for introductory overviews, we will here consider the micro-macro unit-sphere-model developed by Miehe and co-workers [19] since it has proven to perform excellently in reproducing the complex behaviour of elastomers. More detailed theoretical and mathematical derivations of the affine 21-chain model can be found in Lulei [20] and Göktepe [21].

The macroscopic free energy density Ψ of this model is defined as the weighted discrete average of the microscopic free energies φ_i of 21 chains, i.e.

$$\Psi = n \sum_{i=1}^{21} w_i \varphi_i(\lambda_i), \tag{22}$$

where the parameter n denotes the number of chains per unit volume, λ_i is the stretch of the ith chain and the w_i are weighting factors. The chains are assumed to be oriented along certain directions $\boldsymbol{t}_i$ which are chosen such that a normal distribution over the unit sphere is assured. The chain stretches λ_i are related to the macroscopic strain via

$$\lambda_i(\boldsymbol{C}) = \sqrt{\boldsymbol{C} : [\boldsymbol{t}_i \otimes \boldsymbol{t}_i]}. \tag{23}$$

Concerning the energy φ_i of the chain oriented along $\boldsymbol{t}_i$ the model incorporates non-Gaussian statistics for a random walk chain consisting of N identical segments as has been introduced by Kuhn and Grün [22], i.e.

$$\varphi_i\left(\lambda_i^r\right) = k\Theta N \left[\lambda_i^r \mathcal{L}^{-1}\left(\lambda_i^r\right) + \ln \frac{\mathcal{L}^{-1}\left(\lambda_i^r\right)}{\sinh \mathcal{L}^{-1}\left(\lambda_i^r\right)} \right], \tag{24}$$

where $\lambda_i^r = \lambda_i / \sqrt{N}$ denotes the relative chain stretch, k, Θ are Boltzmann's constant and absolute temperature, respectively, and $\mathcal{L}(\bullet) = \coth(\bullet) - 1/(\bullet)$ is Langevin's function. Since the inversion of the latter is not trivial one often substitutes $\mathcal{L}^{-1}$ by the following Padé approximation:

$$\gamma_i := \mathcal{L}^{-1}\left(\lambda_i^r\right) \approx \lambda_i^r \frac{3 - (\lambda_i^r)^2}{1 - (\lambda_i^r)^2}. \tag{25}$$

By defining the shear modulus $\mu := nk\Theta$, adding a volumetric energy term as in the Neo-Hookean case and after some rearrangements the free energy density of the 21-chain model finally reads

$$\Psi(\boldsymbol{C}, J) = \sum_{i=1}^{21} \mu N w_i \left[\gamma_i \lambda_i^r + \ln \frac{\gamma_i}{\sinh \gamma_i} \right] + \frac{1}{2}\kappa (\ln J)^2 - \mu \ln J. \tag{26}$$

The coefficients w_i and the direction vectors $\boldsymbol{t}_i$ required in Eq. (26) go back to the work of Bažant and Oh [23] and are repeated in the Appendix for the sake of completeness.

As in the previous subsection the curing simulation framework requires the computation of the current stiffness and tangent operators. Application of Eq. (3) to (26) yields

$$\mathbb{C}^{n+1} = \sum_{i=1}^{21} w_i \frac{4\mu^{n+1} N^{n+1}}{\left[N^{n+1} - \lambda_i^2\right]^2} [\boldsymbol{t}_i \otimes \boldsymbol{t}_i \otimes \boldsymbol{t}_i \otimes \boldsymbol{t}_i] + \kappa^{n+1} \mathbb{A} - 2\left[\mu^{n+1} - \kappa^{n+1} \ln J\right] \mathbb{B}, \tag{27}$$

which contains three cure dependent parameters, namely the *network parameter* N^{n+1} denoting the number of segments per chain as well as the bulk and shear modulus κ^{n+1} and μ^{n+1}, respectively, whereas the latter includes the number of chains per unit volume n^{n+1}, i.e. a second network parameter. For a detailed derivation of the first part of this stiffness operator the interested reader is refered to [20]. Another partial derivative with respect to $\boldsymbol{C}$ provides the current tangent operator

$$\mathfrak{A}^{n+1} = \frac{\partial \mathbb{C}^{n+1}}{\partial \boldsymbol{C}} = \sum_{i=1}^{21} w_i \frac{8\mu^{n+1} N^{n+1}}{\left[N^{n+1} - \lambda_i^2\right]^3} [\boldsymbol{t}_i \otimes \boldsymbol{t}_i \otimes \boldsymbol{t}_i \otimes \boldsymbol{t}_i \otimes \boldsymbol{t}_i \otimes \boldsymbol{t}_i] + \kappa^{n+1}\left[\mathfrak{B} + 2 \ln J \mathfrak{C} + \mathbb{B} \otimes \boldsymbol{C}^{-1}\right] - 2\mu^{n+1} \mathfrak{C}, \tag{28}$$

with the abbreviations $\mathbb{B}$, $\mathfrak{B}$, $\mathfrak{C}$ as defined in Sect. 4.1.

5 Temporally evolving material parameters

The simulation approach for materials undergoing curing processes as introduced above is intrinsically dependent on the availability of the temporal evolutions experienced by the governing parameters. Usually, such data has to be determined experimentally in a series of tests with materials in different stages of curing. From the literature, e.g. [24,25], it is known that, after the gel point, stiffness parameters like the shear modulus increase drastically following an exponential saturation function of decreasing slope until the fully cured state is reached. A simple expression describing such a behaviour is

$$\mu(t) = \mu_0 + [\mu_\infty - \mu_0][1 - \exp(-\kappa_\mu t)], \tag{29}$$

whereas the initial and final values μ_0 and μ_∞ as well as the curvature parameter κ_μ are required. Figure 1 (left) depicts a corresponding example. As an alternative it is common practice to use formulations in terms of the degree of cure α instead of time, which has some advantages if thermal dependencies are considered. For the sake of simplicity the

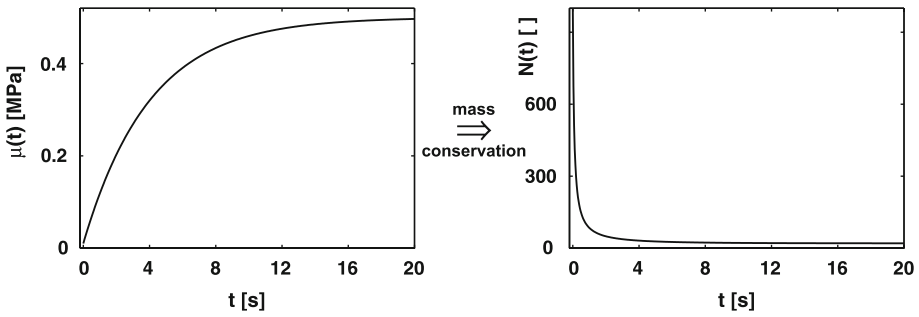

Fig. 1 Evolution of shear modulus $\mu(t)$ (*left*) with $[\mu_0, \mu_\infty, \kappa_\mu] = [0.01\,\text{MPa}, 0.5\,\text{MPa}, 0.25\,\text{s}^{-1}]$ and resulting evolution of the number of chain segments (*right*) with $N_0 = 1{,}000$

following considerations utilise arbitrarily chosen parameter evolutions of the above type since real material data has not been available and is not necessary to demonstrate the properties of our simulation approach.

In case of micromechanically motivated constitutive models like the 21-chain model, the increase in stiffness according to Eq. (29) poses a constraint on the relation between the network parameters n (number of chains per unit volume) and N (number of segments per chain). The conservation of mass requires that the product of chains per unit volume and segments per chain has to be constant during the whole (isothermal) curing process. Thereby, a constant mass/length of the segments is assumed, as well as a sufficient size of the unit volume in a sense that the curing progress does not change the overall number of segments present in this volume. The prescribed evolution of the shear modulus therefore leads to an equation for the current number of segments $N(t)$ since $\mu(t) = n(t)k\Theta$:

$$\begin{aligned} &\text{mass conservation:} \quad n(t)N(t) = n_0 N_0 \quad \forall t \\ \Rightarrow \quad &\mu_0 = n_0 k\Theta = \frac{n(t)N(t)}{N_0} k\Theta = \mu(t)\frac{N(t)}{N_0} \\ \Rightarrow \quad &N(t) = \frac{\mu_0 N_0}{\mu(t)}, \end{aligned} \tag{30}$$

i.e. the necessary parameter evolutions for the 21-chain model can be calculated by prescribing the constants of the exponential saturation function for the shear modulus $(\mu_0, \mu_\infty, \kappa_\mu)$ together with some initial number of segments per chain N_0. The $N(t)$-curve for $N_0 = 1{,}000$ as resulting from the above $\mu(t)$ is plotted in Fig. 1 (right). Similar evolution equations for the material parameters have been used by Dal and Kaliske [26] to assure the conservation of mass in modelling the physical ageing of rubbery polymers.

6 Numerical examples

A number of numerical examples is presented in this section to demonstrate that the proposed simulation framework can reproduce the mechanical behaviour of polymers during isothermal curing, which is, in particular, characterised by a gain in stiffness and a stress rate of zero in case that the strain rate becomes zero. All simulations have been performed using a research-based in-house finite element code that has been extended by the constitutive relations and tangent operators summarised in Sects. 4.1 and 4.2. First, some one-dimensional examples reflect the behaviour of a single eight-noded brick element for a prescribed uniaxial stretch history and parameter evolution. Next, some three-dimensional simulations are presented to demonstrate the influence that different curing rates exert on the material response. For the sake of simplicity, the bulk modulus evolution has always been calculated from the current shear modulus via $\kappa(t) = \frac{2\mu(t)[1+\nu]}{3[1-\nu]}$ by assuming a constant Poisson's ratio $\nu = 0.35$.

6.1 One-dimensional examples

First, a simple uniaxial tension test is simulated using a single finite element to check whether the proposed finite strain curing models will predict the gain in stiffness during the advancement of curing and provide a correct behaviour in case the strain rate becomes zero. To this end a three phase deformation is applied consisting of a linear increase to $\lambda = 1.05$ (macroscopic stretch, not chain stretch) within the first five seconds which is followed by fourty seconds holding and another linear increase to $\lambda = 1.1$ during the last five seconds, cf. Fig. 2.

Both the Neo-Hooke and the 21-chain curing model are used with a prescribed exponential saturation function for

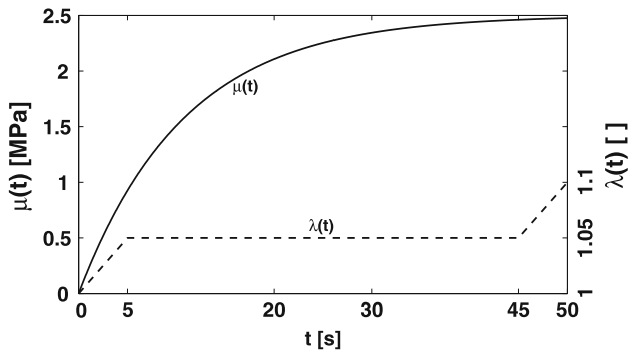

Fig. 2 Load history $\lambda(t)$ and shear modulus evolution $\mu(t)$ according to Eq. (29) with $[\mu_0, \mu_\infty, \kappa_\mu] = [0.0001\,\text{MPa}, 2.5\,\text{MPa}, 0.0925\,\text{s}^{-1}]$, applied to the Neo-Hooke and 21-chain curing model ($N(t)$ as in Eq. (30) with $N_0 = 2 \cdot 10^6$)

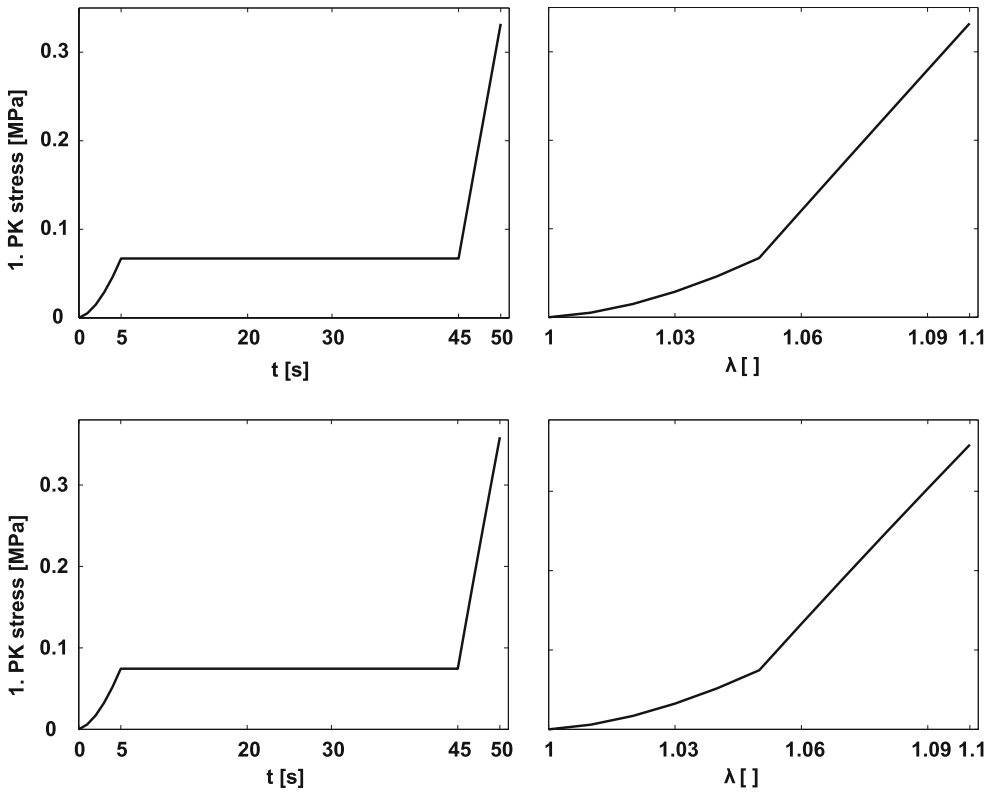

Fig. 3 Elastic curing using the Neo-Hooke (*top*) and 21-chain (*bottom*) model, Piola stress vs. time and stretch

the evolution of the shear modulus, also depicted in Fig. 2. The resulting stress responses versus time and stretch are given in Fig. 3. The physical observation that the stiffness increase during curing has no impact on the stress response of a constant deformation state is correctly reproduced, which is reflected by the constant lines between 5 and 45 s (left-hand plots) and, implicitly, by the kinks at $\lambda = 1.05$ that stem from the continuous increase of μ (right-hand side curves). Furthermore, the initially fast growing shear modulus leads to a nonlinear stress growth during the first five seconds, whereas the behaviour is almost linear with high stiffness at the end since the saturation value for μ has been reached meanwhile.

Note that the 21-chain model responds with a slightly higher maximum stress after 50 s, although the applied deformation seems moderate enough to avoid the dramatic stiffness increase usually induced by the Langevin function at large strains. This misestimation is clarified if the decrease of the number of chain segments N from 2×10^6 at the beginning down to about 80 at the end is considered, i.e. the chains become short enough to enter the nonlinear range near the locking stretch, even if the macroscopic stretch is only 10%.

6.2 Three-dimensional examples

To prove the correct behaviour of our curing models for real three-dimensional structures we first consider a homogeneous block having dimensions of $20 \times 7 \times 3\,\text{mm}^3$ and being discretised by 100 eight-noded brick elements as depicted in Fig. 4a. Boundary conditions and loading are such that a homogeneous uniaxial tension state is achieved, whereas the block is stretched up to six hundred percent, cf. Fig. 4b,c.

Four different parameter evolutions are applied to both the Neo-Hooke and the 21-chain model to clarify the influence that the rate of the curing process exerts on the mechanical responses. In detail we compare a fully cured, very stiff material with an uncured, very soft material as well as two materials with different curing rates, i.e. a large and a small κ_μ. The parameters used are ($[\mu] = \text{MPa}$, $[\kappa_\mu] = \text{s}^{-1}$):

Neo-Hooke:

uncured: $\mu = 0.05$

cured: $\mu = 0.3$

slow: $[\mu_0, \mu_\infty, \kappa_\mu] = [0.05, 0.3, 0.0278]$

fast: $[\mu_0, \mu_\infty, \kappa_\mu] = [0.05, 0.3, 0.0458]$

21-chain:

uncured: $\mu = 0.01\,,\ N = 6000$

cured: $\mu = 0.3\,,\ N = 200$

slow: $[\mu_0, \mu_\infty, \kappa_\mu, N_0] = [0.01, 0.3, 0.0278, 6000]$

fast: $[\mu_0, \mu_\infty, \kappa_\mu, N_0] = [0.01, 0.3, 0.0458, 6000]$.

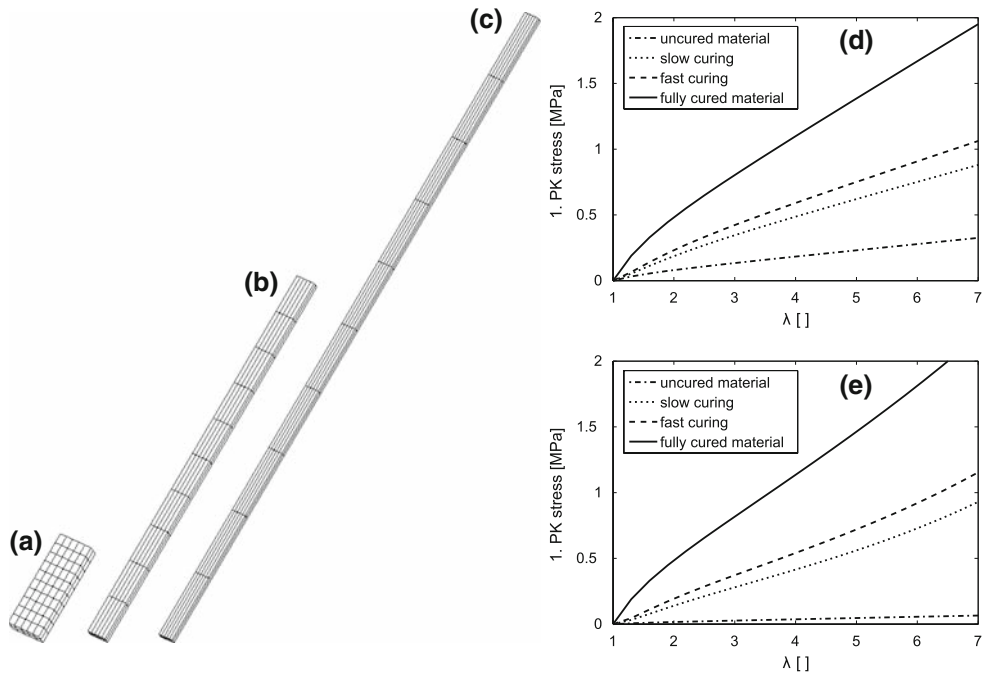

Fig. 4 Three-dimensional block undergoing large deformations. **a** undeformed geometry, **b,c** three and six hundred percent of stretch. Stress responses for uncured, slow and fast curing and fully cured **d** Neo-Hooke and **e** 21-chain material

The results are illustrated in Fig. 4d,e. For very large deformations, the stress-stretch curves of the 21-chain model correctly reproduce the characteristic S-shape, which is not observable in the Neo-Hooke case. The differences between the particular curing regimes are as expected, i.e. higher curing rates yield much stiffer responses.

Finally, a three-dimensional plate with a hole in its center is considered to present an example with inhomogeneous stress distribution under load. Its dimensions are $60 \times 12 \times 2\,\text{mm}^3$ and the hole has a diameter of 6 mm. The plate is discretised by 544 eight-noded hexagonal elements and is supported as depicted in Figs. 5, and 6a. Force increments of 0.0093 N (Neo-Hooke model) and 0.00955 N (21-chain model) are applied at the upper edge nodes to achieve elongations in x-direction. While being loaded, the specimen undergoes elastic curing, whereas

$$[\mu_0, \mu_\infty, \kappa_\mu] = [0.001, 0.5, 0.25]$$

has been chosen for the Neo-Hooke and

$$[\mu_0, \mu_\infty, \kappa_\mu, N_0] = [0.001, 0.5, 0.25, 1 \cdot 10^5]$$

for the 21-chain elastic curing model. Figures 5, and 6b,c depict the resulting deformations and Cauchy stresses in x-direction after five tensile and another five compressive loadsteps. First, tensile stresses and a significant deformation arise, cf. Figs. 5 and 6b while after the second five loadsteps of equal magnitude but reverse direction, the plate is stress-free but, due to the interim stiffness increase, still deformed, cf. Figs. 5, and 6c.

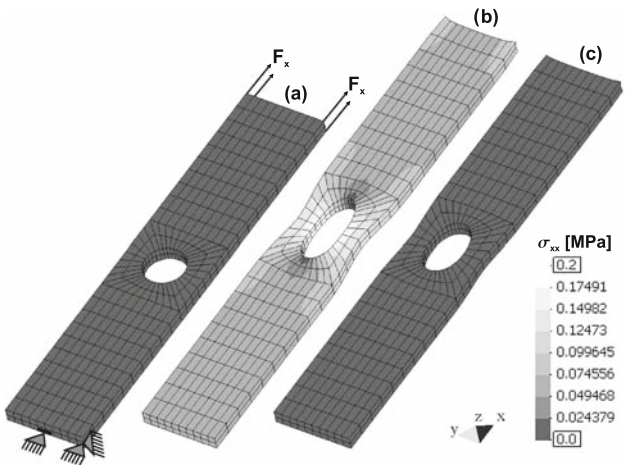

Fig. 5 Inhomogeneous 3d-example, Neo-Hooke elastic curing model, **a**: initial configuration, bearing and loading, **b**: deformation and Cauchy stress after five loadsteps $\Delta F_x = 0.0093\,\text{N}$, **c**: stress-free but still deformed (due to stiffness gain) after five reverse loadsteps $\Delta F_x = -0.0093\,\text{N}$

7 Conclusion and outlook

This contribution proposes a three-dimensional, thermodynamically consistent framework for the simulation of polymeric materials undergoing curing processes and finite

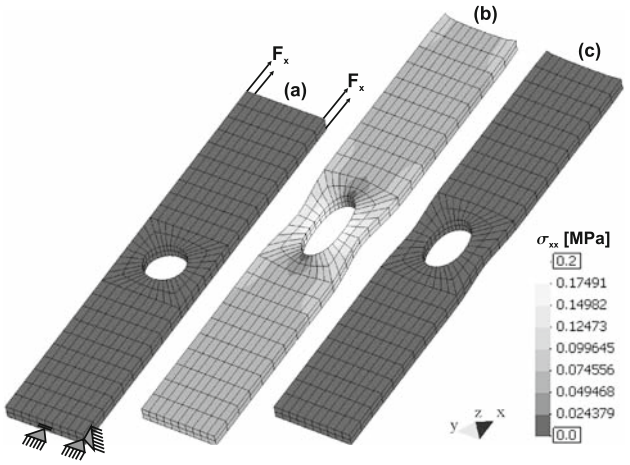

Fig. 6 Inhomogeneous 3d-example, 21-chain elastic curing model, **a**: initial configuration, bearing and loading, **b**: deformation and Cauchy stress after five loadsteps $\Delta F_x = 0.00955\,\mathrm{N}$, **c**: stress-free but still deformed (due to stiffness gain) after five reverse loadsteps $\Delta F_x = -0.00955\,\mathrm{N}$

deformations. Based on some elementary rheological considerations the general equations for stress update and tangent operator as required for a finite element implementation are derived. With this at hand, both phenomenologically and micromechanically motivated elastic polymer models are utilised. The numerical examples demonstrate that the developed approach is suitable to correctly reproduce the relevant phenomena observable in curing polymers. Nonetheless, some restrictions like the assumption of constant temperature and the purely phenomenological character of the presented approach should and will be subject of further investigation. Especially the extension towards viscoelasticity and the consideration of shrinkage effects is going to be dealt with in Part II of this work.

Acknowledgments Financial support by the Rhineland-Palatinate Graduate School 'Engineering Materials and Processes' as well as by the German Research Foundation (DFG) within the collaborative project PAK 108 are gratefully acknowledged. The authors are indebted to an anonymous reviewer for proposing the appropriate free energy density that has been used to prove thermodynamical consistency of our curing formulation.

Appendix

Coefficients w_i and direction vectors $\boldsymbol{t}_i$ as required in the 21-chain model Eq. (26).

$w_{1\ldots3}$	$= 0.0530428488186$		
$w_{4\ldots9}$	$= 0.0398602952624$		
$w_{10\ldots21}$	$= 0.0501424734974$		
i	t_i^1	t_i^2	t_i^3
1	1	0	0
2	0	1	0
3	0	0	1
4	0.707106781187	0.707106781187	0
5	0.707106781187	−0.707106781187	0
6	0.707106781187	0	0.707106781187
7	0.707106781187	0	−0.707106781187
8	0	0.707106781187	0.707106781187
9	0	0.707106781187	−0.707106781187
10	0.387907304067	0.387907304067	0.836095596749
11	0.387907304067	0.387907304067	−0.836095596749
12	0.387907304067	−0.387907304067	0.836095596749
13	0.387907304067	−0.387907304067	−0.836095596749
14	0.387907304067	0.836095596749	0.387907304067
15	0.387907304067	0.836095596749	−0.387907304067
16	0.387907304067	−0.836095596749	0.387907304067
17	0.387907304067	−0.836095596749	−0.387907304067
18	0.836095596749	0.387907304067	0.387907304067
19	0.836095596749	0.387907304067	−0.387907304067
20	0.836095596749	−0.387907304067	0.387907304067
21	0.836095596749	−0.387907304067	−0.387907304067

References

1. Lion A, Höfer P (2007) On the phenomenological representation of curing phenomena in contiuum mechanics. Arch Mech 59:59–89
2. Adolf DB, Chambers RS (2007) A thermodynamically consistent, nonlinear viscoelastic approach for modeling thermosets during cure. J Rheol 51:23–50
3. Kiasat M (2000) Curing shrinkage and residual stresses in viscoelastic thermosetting resins and composites. Ph.D. Thesis, TU Delft, Netherlands
4. van 't Hof C (2006) Mechanical characterization and modeling of curing thermosets. Ph.D. Thesis, TU Delft, Netherlands
5. Hossain M, Possart G, Steinmann P (2009) A small-strain model to simulate the curing of thermosets. Comput Mech 43(6):769–779
6. Adolf DB, Martin JE (1996) Calculation of stresses in crosslinking polymers. J Compos Mater 30:13–34
7. Adolf DB, Chambers RS (1997) Verification of the capability for quantitative stress prediction during epoxy cure. Polymer 38:5481–5490
8. Adolf DB, Martin JE, Chambers RS, Burchett SN, Guess TR (1998) Stresses during thermoset cure. J Mater Res 13:530–550
9. Adolf DB, Chambers RS, Caruthers JM (2004) Extensive validation of a thermodynamically consistent, nonlinear viscoelastic model for glassy polymers. Polymer 45:4599–4621
10. Haupt P, Lion A (2002) On finite linear viscoelasticity of incompressible isotropic materials. Acta Mech 159:87–124
11. Lion A (1998) Thixotropic behaviour of rubber under dynamic loading histories: experiments and theories. J Mech Phys Solids 46:895–930
12. Lion A (1997) On the large deformation behaviour of reinforced rubber at different temperatures. J Mech Phys Solids 45:1805–1834
13. Retka J, Höfer P (2007) Numerische Simulation aushärtender Klebstoffe. Diploma Thesis, Universität der Bundeswehr München
14. Truesdell C, Noll W (1992) The non-linear field theories of mechanics. Springer, Berlin
15. Bonet J, Wood RD (1997) Nonlinear continuum mechanics for finite element analysis. Cambridge University Press, London
16. Wriggers P (2008) Nonlinear finite element methods. Springer, Berlin
17. Boyce MC, Arruda EM (2000) Constitutive models of rubber elasticity: a review. Rubber Chem Technol 73:504–523
18. Marckmann G, Verron E (2006) Comparison of hyperelastic models for rubber-like materials. Rubber Chemistry Technol 79:835–858

19. Miehe C, Göktepe S, Lulei F (2004) A micro-macro approach to rubber-like materials: Part-I. The non-affine micro-sphere model of rubber elasticity. J Mech Phys Solids 52:2617–2660
20. Lulei F (2002) Mikromechanisch motivierte Modelle zur Beschreibung finiter Deformationen gummiartiger Polymere: Physikalische Modellbildung und Numerische Simulation. Ph.D. Thesis, Institut für Mechanik (Bauwesen), University of Stuttgart
21. Göktepe S (2007) Micro-macro approaches to rubbery and glassy polymers: Predictive micromechanically-based models and simulations. Ph.D. Thesis, Institüt für Mechanik (Bauwesen), University of Stuttgart
22. Kuhn W, Grün F (1942) Beziehungen zwischen elastischen Konstanten und Dehnungsdoppelbrechung hochelastischer Stoffe. Kolloid-Zeitschrift 101:248–271
23. Bažant ZP, Oh BH (1986) Efficient numerical integration on the surface of a sphere. Zeitschrift für angewandte Mathematik Mechanik 66:37–49
24. Ruiz E, Trochu F (2005) Thermomechanical properties during cure of glass-polyester RTM composites: elastic and viscoelastic modeling. J Compos Mater 39:881–916
25. Lange J (1999) Viscoelastic properties and transitions during thermal and UV cure of a methacrylate resin. Polym Eng Sci 39:1651–1660
26. Dal H, Kaliske M (2009) A micro-continuum-mechanical material model for failure of rubber-like materials: application to ageing induced fracturing. doi:10.1016/j.jmps.2009.04.007